Applied Catalysis B: Environmental 86 (2009) 145–151

Contents lists available at ScienceDirect

Applied Catalysis B: Environmental

journal homepage: www.elsevier.com/locate/apcatb

Synthesis of visible light-active nanostructured TiO_x ($x < 2$) photocatalysts in a flame aerosol reactor

Swapnil Y. Dhumal [a], Tyrone L. Daulton [b,c], Jingkun Jiang [a,c], Bamin Khomami [a,1], Pratim Biswas [a,c,*]

[a] Department of Energy, Environmental, and Chemical Engineering, One Brookings Drive, Campus Box 1180, Washington University in St. Louis, St. Louis, MO 63130, USA
[b] Department of Physics, One Brookings Drive, Campus Box 1105, Washington University in St. Louis, St. Louis, MO 63130, USA
[c] Center for Materials Innovation, One Brookings Drive, Campus Box 1105, Washington University in St. Louis, St. Louis, MO 63130, USA

ARTICLE INFO

Article history:
Received 16 April 2008
Received in revised form 28 July 2008
Accepted 7 August 2008
Available online 23 August 2008

Keywords:
Oxygen deficient
Titanium dioxide
Flame aerosol reactor
Visible light photocatalytic activity
Nanoparticle

ABSTRACT

Titanium dioxide is a wide band gap (3.2 eV) semiconductor which is photo-active when irradiated with UV light. For wider scale use of TiO_2 as a photocatalyst, its activity needs to be extended to the visible light region (constituting 45% of total incident solar energy). A diffusion flame aerosol reactor (FLAR) with an oxygen lean environment in the particle formation zone has been used to synthesize oxygen deficient titanium suboxide (TiO_x with $x < 2$) nanoparticles. Using a standard-based electron energy loss spectroscopy (EELS) technique, the non-stoichiometry (x in TiO_x) in the flame synthesized particles has been quantified with high accuracy (uncertainty less than 3%). Under an oxygen lean environment in the particle formation zone, the non-stoichiometry in the TiO_x particles is a function of the flame temperature. The value of x in the flame synthesized TiO_x nanoparticles is in the range of $1.88 < x < 1.94$. Diffuse reflectance spectra confirmed that the oxygen deficient TiO_x particles absorbed visible light. Visible light activity of the TiO_x particles is demonstrated by photocatalytic degradation of methyl orange solution under visible light illumination.

1. Introduction

Titanium dioxide is a widely used photocatalyst in applications ranging from air purification and deodorization, water purification, and self-cleaning coatings on buildings [1–4] because of its low cost and high chemical stability. TiO_2 is a wide band gap (3.2 eV) semiconductor material that shows photocatalytic activity with UV light irradiation, that only constitutes approximately 5% of the total incident solar energy. For efficient use of TiO_2 as a photocatalyst for indoor and outdoor applications, it should absorb visible light, which constitutes approximately 45% of the total incident solar energy. Many strategies have been explored to enhance the light absorption in the visible region. Spectral sensitization of organic dyes chemisorbed or physisorbed on the TiO_2 catalyst surface can extend its photocatalytic activity into the visible region [5,6]. However, this method is not applicable in remediation of polluted aqueous streams because of consumption of the dye molecules in the photocatalytic reaction [7].

Oxygen deficient titanium dioxide, represented as TiO_x with $x < 2$, can absorb visible light as oxygen vacancy energy states are formed at 0.75–1.18 eV below the conduction band minimum [8]. This reduction in the energy required for photoexcitation of electrons in the case of TiO_x makes it possible to absorb visible light and extend the photocatalytic activity of titanium dioxide beyond the ultraviolet regime into the visible region. Breckenridge and Hosler [9] reported light absorption in the visible region in the case of slightly reduced oxygen deficient TiO_2. Recently, Ihara et al. [10] prepared oxygen deficient TiO_2 through a reduction reaction of commercially available TiO_2 powder in a RF H_2 plasma. The oxygen deficient particles showed light absorption in the visible region. However, an industrially scalable process for high throughput synthesis of oxygen deficient TiO_2 is still lacking.

Gas phase flame synthesis route is a continuous one step methodology that can be easily scaled up for high throughput production of nanoparticles. It has been a commercially successful approach, and it is used to produce millions of metric tonnes per year of carbon black and metal oxides [11]. The two most commonly used flame configurations are premixed and diffusion flames. In a premixed flame reactor, the fuel and the oxidizer are mixed prior to exiting the burner. In a diffusion flame reactor, the

* Corresponding author at: Department of Energy, Environmental, and Chemical Engineering, One Brookings Drive, Campus Box 1180, Washington University in St. Louis, St. Louis, MO 63130, USA. Tel.: +1 314 935 5548.
E-mail address: Pratim.Biswas@seas.wustl.edu (P. Biswas).
[1] Present address: Department of Chemical and Bimolecular Engineering, University of Tennessee, Knoxville, TN 37996, USA.

0926-3373/$ – see front matter © 2008 Elsevier B.V. All rights reserved.
doi:10.1016/j.apcatb.2008.08.014

fuel and oxidizer come together by molecular diffusion after exiting the burner [12]. Metal oxide particles of various oxygen stoichiometries can be synthesized in a flame reactor by controlling the fuel to oxygen ratio. Hall et al. [13] synthesized SnO_x (x = 0–2) nanoparticles in a diffusion flame and demonstrated that the value of x increased with a decrease in the fuel to oxygen ratio. TiO_2 has been synthesized in flame reactors [14,15]. Rulison et al. [16] and Wegner and Pratsinis [17] reported formation of oxygen deficient titanium suboxide in flame reactors. However, no detailed studies have been carried out to understand the effect of process parameters on the degree of oxygen deficiency in flame synthesized titanium suboxide particles. Moreover, accurate quantification of the degree of oxygen deficiency in the flame synthesized particles and its effect on light absorption and photocatalytic activity is lacking.

In this paper, results of titanium suboxide particles synthesis in a diffusion flame reactor using titanium tetraisopropoxide (TTIP) as a precursor is reported under various process conditions. An accurate estimation of oxygen nonstoichiometry (x in TiO_x), with an uncertainty of less than 3%, was obtained using electron energy loss spectroscopy (EELS). Visible light photocatalytic activity of the flame synthesized TiO_x nanoparticles was demonstrated by examining the degradation of methyl orange solution under visible light illumination.

2. Experimental

2.1. Particle synthesis

The experimental apparatus is shown in Fig. 1A. The experimental apparatus consisted of a reactant feed system, a co-flow diffusion burner, a flame quenching system, and a collection system. A co-flow diffusion flame aerosol reactor (FLAR) consisting of three concentric stainless steel tubes was used [15]. The outer diameters of the tubes were 12.7, 25.4, and 38.1 mm, with a wall thickness of 0.76 mm. The precursor titanium tetra-isopropoxide (TTIP, 97% Aldrich) was atomized in an in-house made stainless steel atomizer with nitrogen carrier gas. The TTIP liquid delivery rate was approximately 8.0 ml/h, which corresponded to a TiO_2 production rate of 2.15 g/h. The N_2/TTIP stream was introduced through the central tube, while methane flowed through the next annulus, and oxygen through the outermost annulus. The precursor delivery tube to the burner was maintained at 210 °C with a heating coil to ensure complete vaporization of the atomized TTIP droplets. The particles were synthesized at fixed flow rates of N_2/TTIP (3.5 lpm) and methane (0.6 lpm), whereas the oxygen flow rate was varied from 0.8 to 4 lpm (0.8, 1.0, 1.2, 2, and 4 lpm; Table 1). The oxygen flow rates of 0.8 and 1.0 lpm represent fuel rich flame conditions with an equivalence ratio (φ, the quotient of the actual fuel to oxygen ratio divided by the stoichiometric fuel-to-oxygen ratio [13]) >1, whereas the flow rate of 1.2 lpm represents stoichiometric conditions (φ = 1). The oxygen flow rates of 2 and 4 lpm represent fuel lean flame conditions ($\varphi < 1$). All flow rates were precisely controlled by mass flow controllers (MKS Instruments).

The flame length and particle residence time in the flame were controlled with the help of a quench ring (i.d. 1.84 cm), which was placed axially around the flame [15]. The particle composition, size, and crystallinity at a given location can be controlled by varying the position of the quench ring with respect to the burner outlet, the burner to quench ring distance (BQD), as shown in Fig. 1A. Compressed nitrogen with a total flow rate (Q_c) of approximately 25 lpm was introduced radially into the quench ring. The nanoparticles were collected downstream on glass fiber filters, facilitated by a vacuum pump.

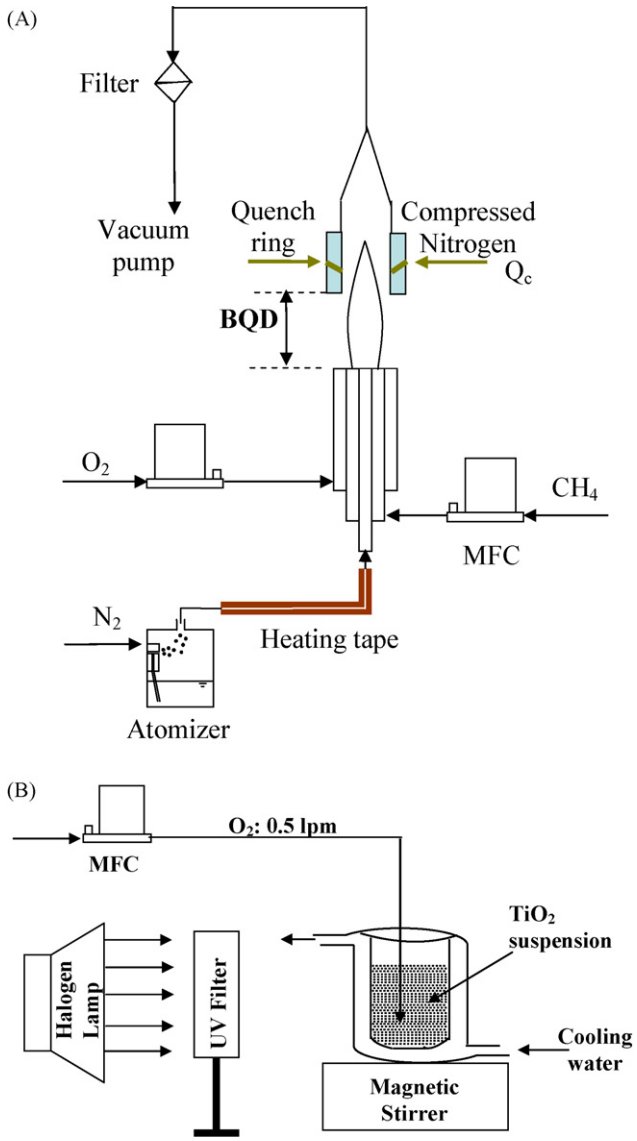

Fig. 1. (A) Schematic diagram of the experimental apparatus for TiO_2 nanoparticle synthesis. (B) Experimental apparatus for studying the photocatalytic degradation of methyl orange under visible light illumination.

Titanium suboxide (TiO_x with $x < 2$) particles can be synthesized at the high temperatures present in a flame aerosol reactor. The high temperature results in the breaking of Ti–O bonds, and subsequently oxygen vacancies are formed by the removal of oxygen from the lattice. The formation of titanium suboxide is favored in an oxygen lean environment in the particle formation zone of the flame reactor. In order to create an oxygen lean environment, oxygen was fed at a controlled rate in the outermost annulus of the diffusion flame reactor, whereas the titanium precursor was fed through the central tube. Since the fuel (CH_4) was fed in the first annulus, the flame front was situated between the first annulus and the outermost annulus, and the oxygen concentration in the particle formation zone (center of the flame) was practically zero.

2.2. Particle characterization

The particle morphology was studied using JEOL JEM-2100F scanning field emission transmission electron microscope (TEM). BET isotherms (Autosorb-1, Quantachrome Instruments) were

Table 1
Summary of the experimental conditions and results

Test number	O_2 flow rate (lpm)	BQD[a] (inch)	O/Ti	SA[b] (m^2/g)	d_{BET}[c] (nm)	d_{XRD}[d] (nm)	d_{TEM}[e] (nm)	k[f] (min^{-1})	k_{SA}[g] ($min^{-1}\ m^{-2}\ mg$)	Y_A[h]
1	0.8	3	1.946	92.68	15.9	11.2	10.9	0.003	0.0324	0.94
2	1.0	3	1.936	84.86	17.4	12.9	13.1	0.0022	0.0259	0.72
3	1.2	3	1.921	81.7	18.3	16.8	14.3	0.002	0.0245	0.58
4	2.0	3	1.897	71.19	21.3	10.5	16.2	0.0018	0.0253	0.51
5	4.0	3	1.886	52.83	29.4	17.3	17.8	0.0014	0.0265	0.47

[a] Quench ring distance from burner outlet.
[b] Specific surface area.
[c] Average particle diameter based on specific surface area measured using BET. For the calculation, the particles were assumed to be spherical.
[d] Average crystallite size based on XRD pattern was determined using Debye–Scherrer formula.
[e] Average particle diameter from TEM.
[f] First-order rate constant for the degradation of methyl orange solution under visible light illumination.
[g] Surface-area-normalized rate constant.
[h] Weight fraction of the anatase phase (Y_A) in the sample is determined using the formula [35] $Y_A = 1/(1 + 1.25(I_R/I_A))$, where I_A and I_R represent the X-ray integrated intensity of the strongest peaks of anatase ($2\theta = 25.5^\circ$ for the (1 0 1) reflection) and rutile ($2\theta = 27.5^\circ$ for the (1 1 0) reflection), respectively.

used to measure the specific surface area of the nanoparticles with nitrogen adsorption at 77 K. The crystalline phase of the synthesized particles was characterized with a Rigaku Geigerflex D-MAX/A X-ray Diffractometer using Cu Kα radiations from $20^\circ < 2\theta < 60^\circ$. The XRD spectra were used to estimate the amount of each crystalline phase in the sample. The light absorption characteristics of the powdered sample were determined using diffuse reflectance spectroscopy.

The non-stoichiometry (x in TiO_x) in the flame synthesized particles was determined using TEM EELS. The non-stoichiometry was expressed in terms of elemental O/Ti ratio, which has a value of 2 for stoichiometric titanium dioxide (TiO_2). A JEOL JEM-2000FX TEM operating at E_o = 200 KeV with a LaB_6 electron source was used for the EELS analysis. The EELS spectrometer (Gatan PEELS Model 666) was calibrated to yield 855.00 ± 0.02 eV for the energy of the Ni-L_3 edge maxima of NiO (e.g., see [18]). The reported calibration error is based on the standard error of the mean of 35 measurements. The following conditions were used during collection of EELS spectra: desaturated filament (to reduce possible specimen charging effects and increase energy resolution), an illumination angle $2\alpha < 5.0 \pm 0.3$ mrad, a collection angle of $2\beta = 6.3 \pm 0.3$ mrad, a 1 mm diameter entrance aperture, and an energy dispersion of 0.2 eV/channel. Three spectra were collected in rapid succession for each acquisition series: a zero-loss, Ti-L/O-K core-loss, and a second zero-loss spectrum. The energy scale of the core-loss spectra was calibrated using the drift-tube offset that was applied to the core-loss spectra and the mean position of the two zero-loss peaks (collected with drift-tube set to zero). The difference in energy of two zero-loss peaks represented the calibration error due to energy drift.

2.3. Determination of photocatalytic activity

The visible light photocatalytic activity of the oxygen deficient titanium dioxide nanoparticles was tested by degradation of methyl orange solution (5 mg/l) in a illuminated Pyrex glass reactor (Fig. 1B). The reactor was maintained at room temperature by circulating water. The solution was illuminated with a 500 W halogen lamp. The UV light from the lamp was blocked by using a UV cut off filter. The Pyrex glass and the circulating water further ensured removal of any radiation below 300 nm and the IR fraction of the light. The powder was suspended in the solution with the help of a magnetic stirrer. The photocatalyst concentration used in all the tests was 0.4 g/L. Oxygen (0.5 lpm) was bubbled through the solution for the entire duration of the experiment. Samples were taken periodically from the reactor, followed by centrifugation and filtration using a 0.2 μm syringe filter to remove the suspended particles. The concentrations of methyl orange solution in the samples collected at different times were obtained by measuring the absorption at a wavelength of 460 nm using a UV–vis spectrophotometer and the absorption data was converted into concentration with a calibration curve. For comparison, the visible light photocatalytic activity of commercial titanium dioxide powder (Degussa P-25) was tested.

3. Results and discussion

Oxygen deficient titanium suboxide nanoparticles were synthesized in a diffusion flame reactor by creating an oxygen lean environment in the particle formation zone. The as produced particles were in an aggregated state with primary particle sizes in the range of ~15–25 nm (Fig. 2). The specific surface area of the particles, synthesized at a BQD of 3 in., decreased with the increase in oxygen flow rate (Table 1). This finding was attributed to the higher flame temperatures encountered by the particles at higher oxygen flow rates (Fig. 3). Average particle size based on BET specific surface area measurements, XRD peak broadening (the largest anatase peak), and TEM measurements are also reported in Table 1. The average particle size based on BET measurements is calculated assuming spherical and unagglomerated particles. Therefore, in the case of agglomerated particles, the particle size based on BET measurements will be greater than the actual particle size. This explains the difference in the average

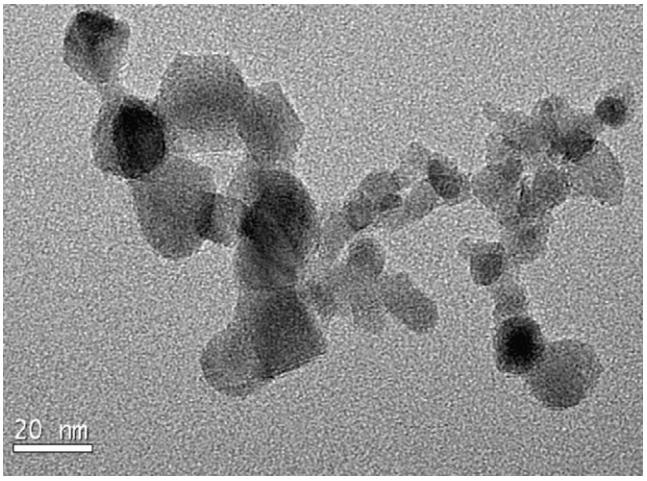

Fig. 2. TEM image of titanium suboxide particles synthesized in the flame at oxygen flow rate of 2 lpm.

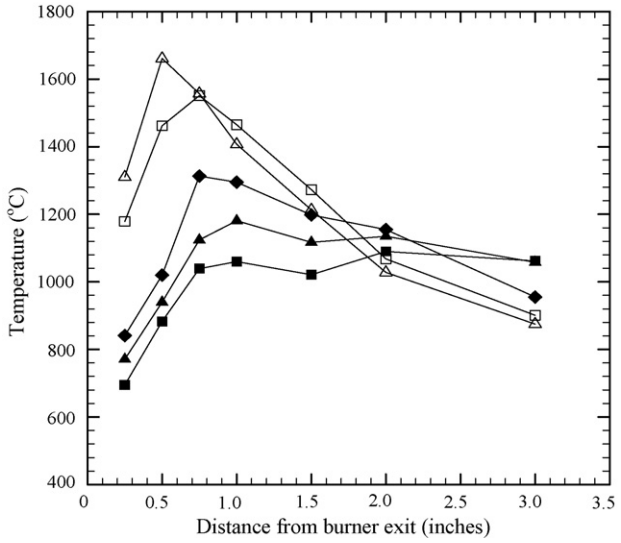

Fig. 3. Temperatures at the center of the flame with oxygen flow rates of 0.8 lpm (■), 1 lpm (▲), 1.2 lpm (◆), 2 lpm (□) and 4 lpm (△) without the quenching ring.

particle size based on BET and XRD measurements listed in Table 1. The axial center-line temperature distribution in the flame was measured using a type B Pt–Rh thermocouple and corrected for radiation losses. Fig. 4 shows the XRD spectra of the particles synthesized at different oxygen flow rates, with a BQD of 3 in. Under the set of conditions used in this study, a mixture of anatase and rutile phases is obtained. The anatase fraction in the mixture decreased with an increase in oxygen flow rate (Table 1). This observation was attributed to an increase in flame temperature with an increase in oxygen flow rate since the anatase to rutile phase transformation is favored by high temperatures.

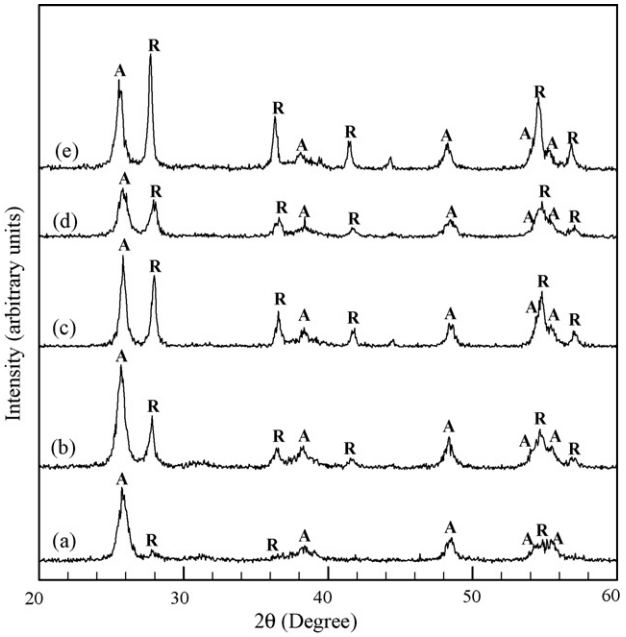

Fig. 4. X-ray diffraction spectra of particles synthesized at O_2 flow rate of (a) 0.8 lpm; (b) 1 lpm; (c) 1.2 lpm; (d) 2 lpm; (e) 4 lpm; with burner to quench ring distance (BQD) of 3 in. [A and R correspond to anatase and rutile phases, respectively].

3.1. Oxygen deficiency (x in TiO_x)

The O/Ti elemental ratios were determined from the EELS Ti L-edge and O-K edge core-loss intensity, I_i, integrated over the energy window Δ_i, as well as the partial cross-sections for inner-shell scattering, σ_i, integrated over the same energy windows. For $\alpha \ll \beta$ these quantities are related by

$$\frac{O}{Ti} = \left(\frac{I_O(E_o, \alpha, \beta, \Delta_O)}{I_{Ti}(E_o, \alpha, \beta, \Delta_{Ti})}\right)\left(\frac{\sigma_{Ti}(E_o, \alpha, \beta, \Delta_{Ti})}{\sigma_O(E_o, \alpha, \beta, \Delta_O)}\right) \quad (1)$$

where E_o is the energy of the incident electron beam, α is the beam convergence angle, and β is the spectrometer collection angle (in general, O and Ti can be any elements).

Ratios of inelastic partial cross-sections can be calculated from theoretical hydrogenic and Hartree–Slater models [19–22] (i.e., standardless method) or determined experimentally from measurements of standards [24] (i.e., "k-factor" approach). Experimentally measured cross-sections are more accurate yielding higher accuracy in the determination of elemental ratios [23–27]. Since high precision is required to distinguish small changes in stoichiometry of TiO_x as a function of synthesis conditions, we quantified the O/Ti ratios in the flame synthesized particles using experimentally measured cross-sections. Using the standard-based technique we were able to measure the O/Ti ratio with an uncertainty of less than 3%.

Seven standards were analyzed: Ti_2O_3, TiO, TiO_2, $TiSiO_4$, $BaTiO_3$, $PbTiO_3$, and $MgTi_2O_5$. All standards were powdered, placed directly on Cu TEM grids coated with holey or lacy amorphous carbon, and analyzed immediately following preparation. For each standard, EELS spectra sets were collected from at least 30 specimen regions (i.e., individual grains or clusters of grains). This allowed the range of possible specimen heterogeneity in the standard to be sampled and this would be reflected in part by the scatter in the data. Spectra sets were processed by standalone software written and compiled specifically for the analysis. In that processing, pre-edge backgrounds were subtracted from both the Ti-$L_{2,3}$ and O-K edges. The background for the edges was approximated by a power law of the form Ae^{-R}, where e is the electron energy loss. From the integrated edge signal and the known O/Ti ratio of the standard, the ratio of inelastic partial cross-sections for inner-shell scattering of Ti and O, σ_O/σ_{Ti}, were then determined. For each standard, the results were averaged (data which deviated from the standard deviation of the mean by greater than a factor of 2.5 were excluded) and reported with the statistical standard error (Fig. 5B). The O/Ti ratio of the unknowns were quantified using the mean ratio of partial cross-sections ($\sigma_O/\sigma_{Ti} = 0.0432 \pm 0.0005$).

For each experimental sample, six replicate EELS spectra sets were collected from each of six different specimen regions (i.e., clusters of grains). The spectra were processed in the same manner as the standards with the only difference that the O/Ti ratio was determined from the integrated edge signal and the experimentally measured ratio of partial cross-sections. For each experimental region, the results from the six replicate measurements were averaged (data which deviated from the standard deviation of the mean by greater than a factor of 2.5 were excluded). The results of the six area measurements for any given sample were averaged (data which deviated from the standard deviation of the mean by greater than a factor of 2.5 were excluded) and reported with the statistical standard error.

Fig. 6 shows the variation of the O/Ti ratio (x in TiO_x) in flame synthesized particles as a function of oxygen flow rate. For all the oxygen flow rates, the BQD was kept constant at 3 in. The O/Ti ratio decreased with the increase in oxygen flow rate, i.e., the oxygen deficiency in the synthesized particles increased with the increase

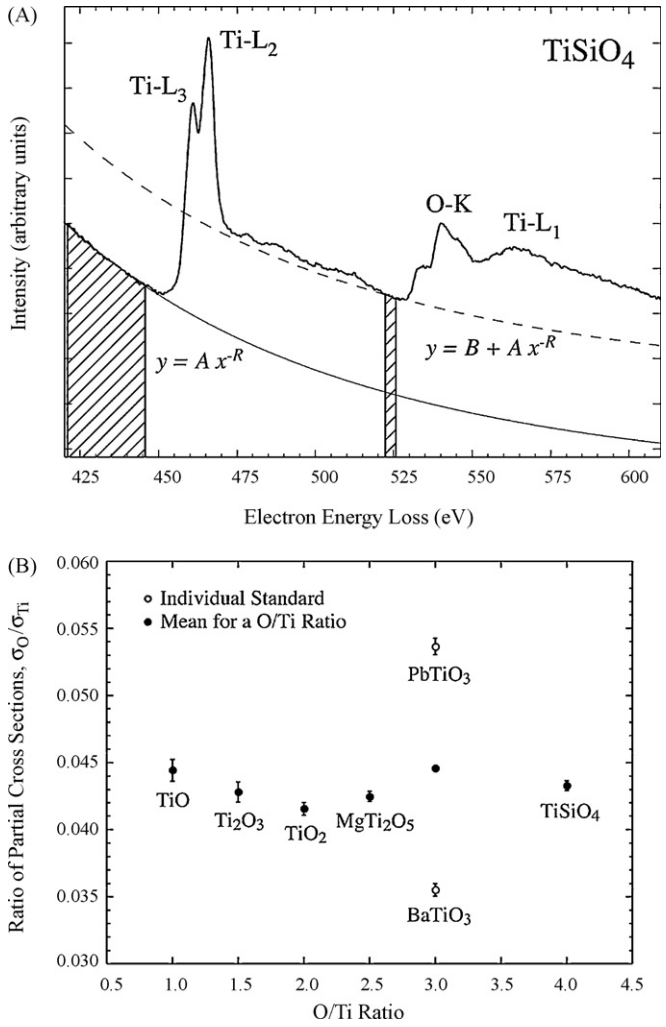

Fig. 5. (A) Electron energy loss spectra of a quantification standard illustrating the inelastic background models subtracted from the Ti-$L_{3,2}$ (solid) and O-K (dashed) edges. Parameters A and R were determined by linear least squares fit to the cross-hatched region immediately preceding the Ti-$L_{3,2}$ edge, and B was determined from the mean counts in the cross-hatched region immediately preceding the O-K edge. (B) Experimentally measured ratios of inelastic partial cross-sections for inner-shell scattering of Ti with respect to O, σ_O/σ_{Ti}: individual standards (open circles) and mean for a particular O/Ti ratio (solid circles). Cross-sections are a function of the following experimental values: E_o, σ, β, and ω (see text for their definition and respective values). The mean cross-section for each O/Ti ratio were averaged yielding $\sigma_{Ti}/\sigma_O = 0.0432 \pm 0.0005$.

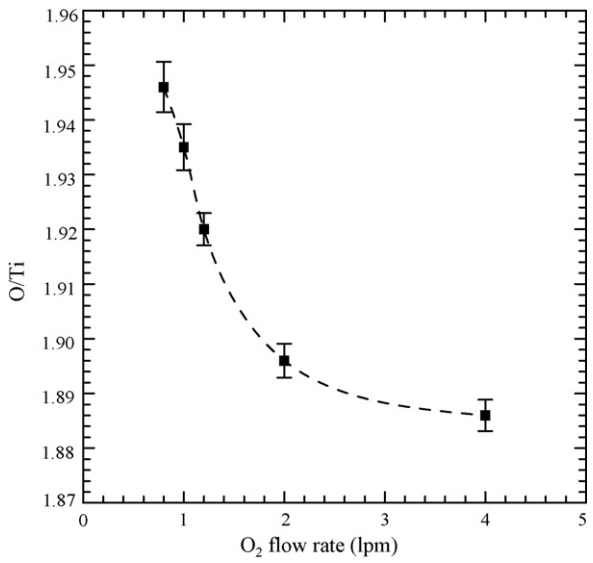

Fig. 6. O/Ti (i.e., x in TiO_x) ratio in the particles collected with BQD = 3 in. as a function of oxygen flow rate [BQD: Burner to quench ring distance]. The dotted curve is a guide to understand the trend.

in oxygen flow rate due to an associated increase of the flame temperature. Increase in the flame temperature represents an increase in the probability of creating oxygen vacancies, and thereby an increase in the degree of oxygen deficiency in the particles. The axial center-line temperature distribution in the flame at different oxygen flow rates is shown in Fig. 3. The flame temperatures were measured without a quenching ring. The flame temperature increases with the increase in oxygen flow, which explains the accompanying increase in oxygen deficiency in Fig. 6. Farther away from the burner outlet (~3 in.), it was observed that the flame temperatures corresponding to high oxygen flow rates (2 and 4 lpm) is lower than the temperatures corresponding to low oxygen flow rates. This reversal in trend could be the result of over-ventilated (oxygen flow of 2 and 4 lpm) versus under-ventilated (0.8 and 1 lpm) flame conditions. Since the ring was used to quench the flow at this location, this reversal in temperature versus oxygen flow trend should have no significant effect on the creation of oxygen vacancies at a given oxygen flow rate. The flame temperature increases with the increase in oxygen flow rate, which explains the accompanying increase in oxygen deficiency. Particles were also synthesized at an oxygen flow rate of 4 lpm without a quenching ring. In this case, the particles were collected at ~6 in. from the burner outlet. The particles synthesized at 4 lpm without the quenching ring were stoichiometric (O/Ti = 2), whereas the particles synthesized at 4 lpm with a quenching ring at 3 in. from burner outlet were non-stoichiometric (O/Ti < 2). The formation of stoichiometric TiO_2 particles in the absence of a quenching ring could be attributed to the complete reoxidation of the oxygen deficient particles by the excess supplied oxygen (an oxygen flow rate of 4 lpm represents an over-ventilated flame with $\varphi < 1$). With the help of the quenching ring system, we were able to prevent complete reoxidation of the oxygen deficient particles in the case of the over-ventilated flame due to a rapid decrease in the temperature.

The long-term stability of titanium suboxide particles in ambient atmospheres were studied by exposing the samples synthesized at oxygen flow rate of 4 lpm to outdoor air/sunlight for 90 days. On reanalyzing the suboxide particles the O/Ti ratio changed from 1.886 to 1.915, and stabilized at this value. The slight increase in the O/Ti ratio is probably due to the oxidation of the vacancies present on the surface. The bulk vacancies are kinetically stable to oxidation at room temperature. Thermal treatment however results in complete oxidation, and the suboxide particles were completely oxidized when heated in air at 400° C for 2 h (O/Ti ratio = 2).

3.2. Visible light absorption

The reflectance spectra of the particles synthesized in the flame reactor are shown in Fig. 7. As a reference, the reflectance spectrum of commercially available Degussa P-25 TiO_2 particles is also shown. The stoichiometric (O/Ti = 2) Degussa P-25 particles did not show any absorption in the visible region. The flame synthesized oxygen deficient (O/Ti < 2) particles absorbed light across the entire visible region. This finding is in accordance with the calculated optical absorption spectra of Lin et al. [28], who used the spin-polarized plane-wave pseudopotential method for the calculation of optical

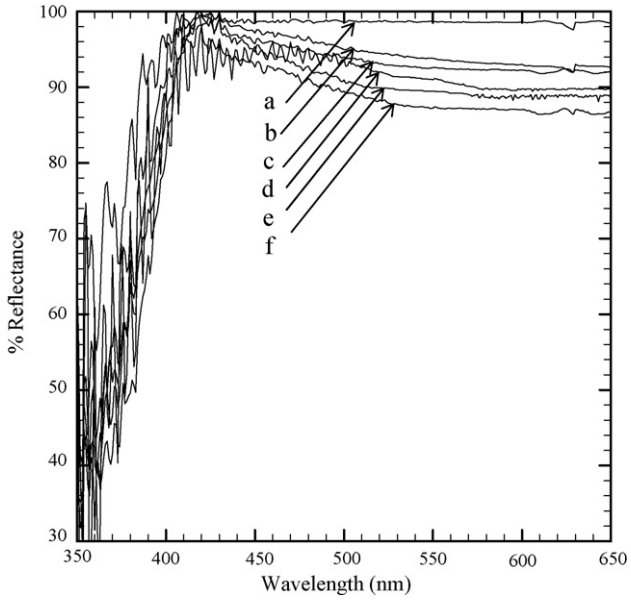

Fig. 7. Diffuse reflectance spectra of (a) commercial TiO_2 particles (Degussa P-25) and (b–f) oxygen deficient particles synthesized in the diffusion flame at different oxygen flow rates with BQD = 3 in. (b: 0.8 lpm; c: 1 lpm; d: 1.2 lpm; e: 2 lpm; f: 4 lpm).

absorption spectra of oxygen deficient TiO_2. Lin et al. [28] showed that the relatively large number of 3d Ti donor states that are present at oxygen deficiency around O/Ti = 1.875 results in strong optical absorption across the entire visible light region. The values of O/Ti in the flame synthesized particles are in the range of 1.88–1.94, which explains the observed visible light absorption for these particles.

3.3. Photocatalytic activity of TiO_x particles

The visible light activity of the TiO_x particles was investigated by photocatalytic degradation of methyl orange solution. The change in methyl orange concentration as a function of time is plotted in Fig. 8. The first-order rate constant k, obtained by fitting the experimental data, is also reported in Table 1. The flame synthesized oxygen deficient particles showed photocatalytic activity under visible light illumination. However, the stoichiometric Degussa P-25 TiO_2 particles did not show any visible light photocatalytic activity. This finding is in accordance with the observed reflectance spectra, where the oxygen deficient particles showed light absorption in the visible region, whereas Degussa P-25 TiO_2 particles did not absorb any visible light. No degradation of methyl orange solution was observed in the absence of particles and with the light on.

The oxygen deficient TiO_x particles synthesized at an oxygen flow rate of 0.8 lpm showed the highest photocatalytic activity, whereas the particles synthesized at 4 lpm showed the lowest activity. Surface area, oxygen deficiency, and crystalline phase composition of the particles influence the photocatalytic activity of the TiO_x particles [29,30]. In a flame, these three parameters vary with the oxygen flow rate (Table 1). In order to factor out the surface area effects, the first-order rate constant (k) was normalized with specific surface area since all the rate measurements were done at constant mass loading. The variation of the surface-area-normalized rate constant (k_{SA}) as a function of O/Ti ratio (x in TiO_x) is shown in Fig. 9. The surface-area-normalized rate constant decreased with the increase in O/Ti ratio (the decrease in oxygen deficiency) up to a value of O/Ti = 1.91, beyond which k_{SA} increased with the O/Ti ratio. This increase in k_{SA} could be the result of an increased anatase fraction in the particles corresponding O/Ti > 1.91. It is commonly believed that the anatase phase of titanium dioxide has higher photocatalytic activity than the rutile phase [3,31,32].

In stoichiometric TiO_2, the valence band is dominated mostly by oxygen 2p states and is filled, whereas the conduction band, comprising mostly of Ti 3d states, is empty. A band gap energy of 3.2 eV in stoichiometric TiO_2, corresponding to a wavelength of 387 nm, does not result in significant absorption of light in the visible region (400–700 nm). When oxygen atoms are removed from stoichiometric TiO_2, there is an excess number of electrons. Cronemeyer [8] demonstrated that in a reduced TiO_2 single crystal, there exist oxygen vacancy states at 0.75–1.18 eV below the conduction band minimum. Introduction of the oxygen vacancy

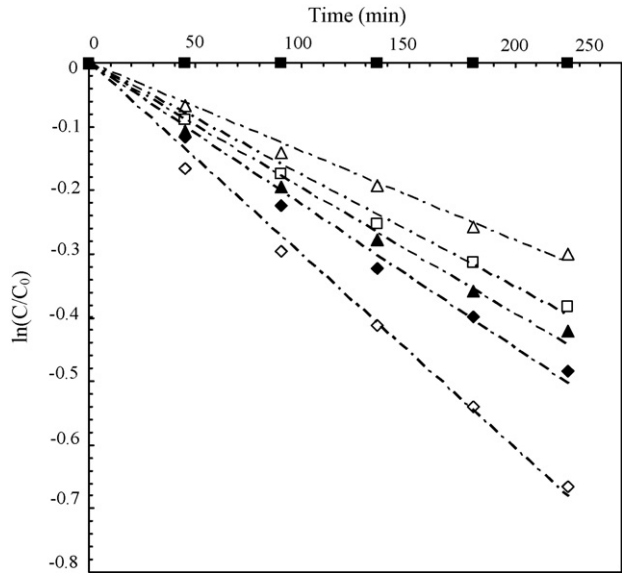

Fig. 8. Visible light photocatalytic degradation of methyl orange solution using the commercial (Degussa P-25) TiO_2 particles (■) and oxygen deficient particles synthesized in the diffusion flame at different oxygen flow rates with BQD = 3 in. [0.8 lpm (◇); 1 lpm (◆); 1.2 lpm (▲); 2 lpm (□); 4 lpm (△)].

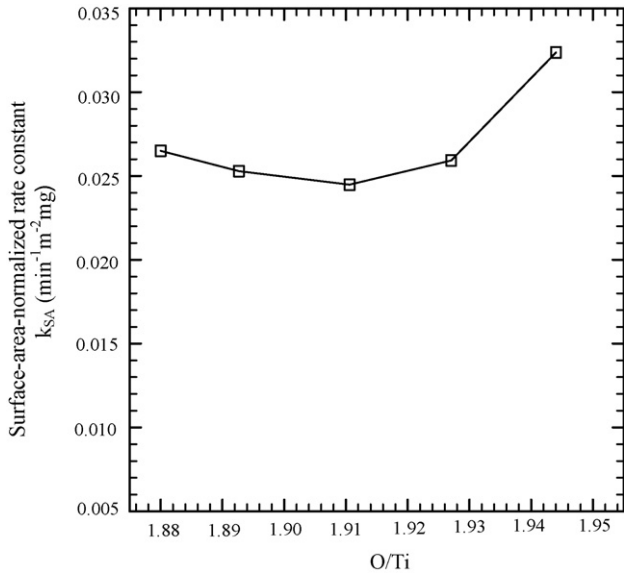

Fig. 9. Surface-area-normalized first-order rate constant (k_{SA}) for visible light photocatalytic degradation of methyl orange solution as a function of O/Ti ratio in particles synthesized in a diffusion flame reactor at different oxygen flow rates with BQD = 3 in. [BQD: Burner to quench ring distance].

states reduce the band gap (2.02–2.45 eV) with respect to the stoichiometric TiO_2, so that photoexcitation of electrons from the valance band can take place with visible light. This is in accord with the experimentally observed reflectance spectra of flame synthesized oxygen deficient particles. It has been argued that these oxygen vacancy states are localized, and due to the low mobility of electrons in these levels, the photodegradation activity will be limited [33]. However, Justica et al. [34], through first principle calculations based on density functional theory, showed that for one vacancy for every 50 oxygen atoms, the defect bands due to oxygen vacancies start overlapping with the conduction band. The vacancy concentration in the oxygen deficient particles synthesized in this work is greater than the value of one vacancy per 50 oxygen atoms. Therefore, overlapping of the bands is most likely taking place in these particles, and is probably responsible for the observed photocatalytic activity in the visible range.

4. Conclusions

A flame aerosol reactor system was developed for the controlled synthesis of visible light-active titanium dioxide photocatalysts. Specifically, oxygen deficient titanium suboxide (TiO_x with $x < 2$) nanoparticles were synthesized in a diffusion flame aerosol reactor by creating an oxygen lean environment in the particle formation zone. An accurate estimation of the non-stoichiometry (x in TiO_x) with an uncertainty of less than 3% was achieved through a standard-based electron energy loss spectroscopy technique. Particles with varied degrees of oxygen deficiency (x in the range of 1.88–1.94) were synthesized by controlling the oxygen flow rate, and thereby the flame temperature. The oxygen deficiency increased with the increase in temperature.

The oxygen deficient particles were able to absorb visible light and showed visible light photocatalytic activity in degradation of methyl orange solution. The commercially available Degussa P-25 TiO_2 particles did not show any visible light absorption, and no photocatalytic activity was observed under visible light illumination. Thus, flame aerosol reactors, under an oxygen lean environment, provide a one step process for high throughput synthesis of nanostructured oxygen deficient titanium suboxide particles for visible light activated applications.

Acknowledgements

This work was partially supported by the Center for Materials Innovation, Washington University, St. Louis, and a grant from DOD MURI Program (#UR 523873).

References

[1] M. Janus, B. Tryba, M. Inagaki, A.W. Morawski, Appl. Catal. B: Environ. 52 (2004) 61–67.
[2] A.G. Agrios, P. Pichat, Rev. Appl. Elect. 35 (2005) 655–663.
[3] O. Carp, C.L. Huisman, A. Reller, Prog. Solid State Chem. 32 (2004) 33–177.
[4] C.B. Almquist, P. Biswas, J. Catal. 212 (2002) 145–156.
[5] O. Ozcan, F. Yukruk, E.U. Akkaya, D. Uner, Appl. Catal. B: Environ. 71 (2007) 291–297.
[6] T. Wu, G. Liu, J. Zhao, H. Hidaka, N. Serpone, J. Phys. Chem. B 102 (1998) 5845–5851.
[7] H. Liu, W. Yang, Y. Ma, J. Yao, Appl. Catal. A: Gen. 299 (2006) 218–223.
[8] D.C. Cronemeyer, Phys. Rev. 113 (1959) 1222–1226.
[9] R.G. Breckenridge, W.R. Hosler, Phys. Rev. 91 (1953) 793–802.
[10] T. Ihara, M. Miyoshi, M. Ando, S. Sugihara, Y. Iriyama, J. Mater. Sci. 36 (2001) 4201–4207.
[11] M.T. Swihart, Curr. Opin. Colloid Interface Sci. 8 (2003) 127–133.
[12] M.R. Zachariah, S. Huzarewicz, J. Mater. Res. 6 (1991) 264–269.
[13] D.L. Hall, A.A. Wang, K.T. Joy, T.A. Miller, M.S. Wooldridge, J. Am. Ceram. Soc. 87 (2004) 2033–2041.
[14] G.X. Yang, H.R. Zhuang, P. Biswas, Nanostruct. Mater. 7 (1996) 675–689.
[15] J. Jiang, D.R. Chen, P. Biswas, Nanotechnology 18 (2007) 285603–285611.
[16] A.J. Rulison, P.F. Miquel, J.L. Katz, J. Mater. Res. 11 (1996) 3083–3089.
[17] K. Wegner, S.E. Pratsinis, AIChE J. 49 (2003) 1667–1675.
[18] T.L. Daulton, B.J. Little, Ultramicroscopy 106 (2006) 561–573.
[19] R.F. Egerton, Ultramicroscopy 3 (1978) 243–251.
[20] R.D. Leapman, P. Rez, D.F. Mayers, J. Chem. Phys. 72 (1980) 1232–1243.
[21] P. Rez, Ultramicroscopy 9 (1982) 283–287.
[22] P. Rez, Ultramicroscopy 28 (1989) 16–23.
[23] J. Auerhammer, P. Rez, F. Hofer, Ultramicroscopy 30 (1989) 365–370.
[24] F. Hofer, Microsc. Microanal. Microstruct. 2 (1991) 215–230.
[25] F. Hofer, B. Luo, Ultramicroscopy 38 (1991) 159–167.
[26] F. Hofer, P. Wilhelm, Ultramicroscopy 49 (1993) 189–197.
[27] F. Hofer, G. Kothleitner, P. Rez, Ultramicroscopy 63 (1996) 239–245.
[28] Z. Lin, A. Orlov, R.M. Lambert, M. Payne, J. Phys. Chem. B 109 (2005) 20948–20952.
[29] J. Jiang, G. Oberdörster, E. Elder, R. Gelein, P. Mercer, P. Biswas, Nanotoxicology 2 (2008) 33–42.
[30] V. Tiwari, J. Jiang, V. Sethi, P. Biswas, Appl. Catal. A: Gen. 345 (2008) 241–246.
[31] E. Thimsen, P. Biswas, AIChE J. 53 (2007) 1727–1735.
[32] E. Thimsen, N. Rastgar, P. Biswas, J. Phys. Chem. C 112 (2008) 4134–4140.
[33] R. Asahi, T. Morikawa, T. Ohwaki, K. Aoki, Y. Taga, Science 293 (2001) 269–271.
[34] I. Justica, C.G. Ordejon, J. Mozos, J. Fraxedas, G. Battiston, R. Gerbasi, A. Figueras, Adv. Mater. 14 (2002) 1399–1402.
[35] R.A. Spurr, H. Meyers, Anal. Chem. 29 (1957) 760–776.